One-Cycle Control for a Double-Input DC/DC Converter

Dongsheng Yang, Min Yang, and Xinbo Ruan, *Senior Member, IEEE*

***Abstract*—In hybrid power systems, the use of a multiple-input converter (MIC) instead of several single-input converters leads to a simpler circuit and lower cost. Energy management is always required for the MICs in order to ensure the highest utilization of renewable energy. The MIC-based hybrid power system is a typical multiple-input multiple-output coupling system, and it has multiple operating modes. As a result, the design of the controllers is very complicated. This paper proposes one-cycle control (OCC) for double-input buck converter (DIBC) to eliminate the interactions of the control loops and, thus, to simplify the design of the controllers. The mode transition circuit is further proposed to realize seamless mode transition, according to the available renewable energy and the output power. Small signal models of DIBC in different operating modes are derived. It can be seen that with OCC, the two control loops are independent of each other, and no current regulator is required. Moreover, the design conditions of the output voltage regulator in different operating modes are the same. As a result, the controller design is greatly simplified. An 800-W prototype has been built and tested in the lab and the experimental results validate the proposed OCC.**

***Index Terms*—Closed loop, hybrid power system, multi-input multi-output (MIMO), multiple-input converter (MIC), one-cycle control (OCC), small signal modeling.**

I. Introduction

MUCH interest has arisen in utilizing renewable energy to curb greenhouse gas emissions and resist climate changes. Compared with traditional fossil fuels, the renewable energy is more environment friendly and sustainable. However, renewable energy sources such as photovoltaic (PV) solar energy and wind energy rely heavily on the climate and weather conditions. As a consequence, the available power is intermittent and stochastic. So, multiple renewable energy sources that are mutually complementary could be combined to maintain continuous power delivery to the load. Such a system is referred to as a hybrid power system. A number of independent single-input converters can be used to interface these renewable energy sources [1]–[3]. Recently, multiple-input converters (MICs) have received increased attention, and they are capable of replacing several single-input converters in order to reduce complexity and the cost of hybrid power systems [4]–[7].

An MIC is capable of converting power from multiple input sources to a common load. Power management is required for an MIC to appropriately distribute the output power to the input sources according to the characteristics of the renewable energy sources, and at the same time regulate the output voltage. Therefore, MIC's control system is composed of one output voltage loop and several input current or input voltage loops. The input current or input voltage loops regulate the currents or voltages of the input sources, and, consequently, regulate the input power of these sources [8]–[11]. Because the input sources share the output filter, these closed loops, including the output voltage loop and the input current or voltage loops, are coupled with each other when the input sources deliver power to the load simultaneously. In addition, the MICs have multiple operating modes at different output power and available renewable energy. So the design of the closed loops is very complicated.

If the effect of the cross-coupling transfer functions is negligible, the regulators can be easily designed in a decoupled manner [12], [13]. However, if their effect is significant, the individual regulators must be designed based on the combined plant. Considering the cross-coupling transfer functions, a design method of the closed loops for the double-input buck converter (DIBC) was proposed in [14]. The DIBC has three operating modes among which only two have a single output voltage closed loop or an output voltage closed loop with an inner input current loop, and the other one has an output voltage closed loop and an input current closed loop, and they are coupled with each other. The output voltage regulator and the input current regulator are first designed independently in the operating mode that contains only a single closed loop or a dual closed loop, and then, the designed regulator parameters are substituted into the other operating mode, which has the coupled closed loops, to check whether the operating mode is stable and the dynamic responses meet the requirements. If not, two regulators should be redesigned until the stability as well as the dynamic responses satisfy the requirements. Thus, this method is a trial and error one and is relatively complicated.

Decoupling matrix is an effective method to deal with the coupling loops, which reduces the original transfer function matrix into a diagonal matrix. As a result, the coupling loops can be treated as a number of single-input single-output control loops and their regulators can be designed independently.

Manuscript received April 6, 2011; revised July 1, 2011; accepted July 31, 2011. Date of current version June 20, 2012. This work was supported by the National Natural Science Foundations of China under Award 50837003 and Award 50807024. Recommended for publication by Associate Editor G. Oriti.

D. Yang and M. Yang are with the Aero-Power Sci-tech Center, College of Automation Engineering, Nanjing University of Aeronautics and Astronautics, Nanjing 210016, China (e-mail: yangdongsheng@nuaa.edu.cn; candy_yangmin@sina.cn).

X. Ruan is with the Aero-Power Sci-tech Center, College of Automation Engineering, Nanjing University of Aeronautics and Astronautics, Nanjing 210016, China, and also with the College of Electrical and Electronic Engineering, Huazhong University of Science and Technology, Wuhan 430074, China (e-mail: ruanxb@nuaa.edu.cn).

Color versions of one or more of the figures in this paper are available online at http://ieeexplore.ieee.org.

Digital Object Identifier 10.1109/TPEL.2011.2164582

Due to the fact that the decoupling matrix highly depends on the original transfer function matrix which is determined by the topology of MIC and controlled variables, different decoupling matrixes have to be introduced when the MIC operates under several operating modes [15]. Moreover, the parameters of the original transfer function will vary with input voltages and load even in the same operating mode [16], [17], so the parameters of the decoupling matrix must be tuned accordingly. Thus, the implementation of the decoupling matrixes is quite difficult.

All the previously mentioned control methods are based on the linear feedback control technique, so they need both the voltage regulator(s) and current regulator(s). In addition, any change of the input source or load must be first sensed as an output change and then corrected by the regulator. This usually means slow response. One-cycle control (OCC) is a kind of nonlinear control technique, which achieves instantaneous dynamic control of the average value of a switched variable. The average value of the switched variable can follow its control reference within a switching cycle and the power perturbations are rejected as well [18]. Another advantage of OCC is that the regulator is not required when the controlled variable is a switched variable that can be controlled directly by OCC [19]. It has been widely applied in dc–dc conversion [20], power amplifier [21], power factor correction [22], active power filter [23], and maximum power point tracking (MPPT) of PV solar energy [24]. It is also desirable for the MIC to avoid the difficulty of designing regulators. The objective of this paper is to employ the OCC for the MICs to improve the dynamic response and reject the perturbations of input sources, and further diminish the interactions among the various control loops.

Taking the DIBC as the example, this paper proposes the OCC method for MICs to simplify the design of the regulators. This paper is organized as follows. Section II illustrates the power management strategy for the DIBC, and two different operating modes are described in detail. Then the implementations of the OCC for the DIBC are proposed in Section III, in which the mode transition circuit is further proposed to realize seamless mode transition. Small signal model of the DIBC with OCC is derived and the regulator design is given in Section IV. In order to verify the effectiveness of OCC and the closed-loops design, an 800-W prototype of DIBC has been built and tested in the lab, and the experimental results are presented in Section V. Finally, conclusions are given in Section VI.

II. Power Management for a DIBC

The DIBC is shown in Fig. 1, where $V_{\rm in1}$ and $V_{\rm in2}$ are the two input sources, Q_1 and Q_2 are the switches, D_1 and D_2 are the freewheeling diodes, L_f is the filter inductor, R_{Lf} is the parasitical resistor of L_f, C_f is the filter capacitor, and R_{cf} is the equivalent series resistor of C_f. Two input sources of DIBC can deliver energy to the load simultaneously or individually.

According to Fig. 1, the output voltage and input currents at steady state are given by

$$V_o = \bar{v}_{AB} = D_{y1}V_{\rm in1} + D_{y2}V_{\rm in2} \tag{1}$$

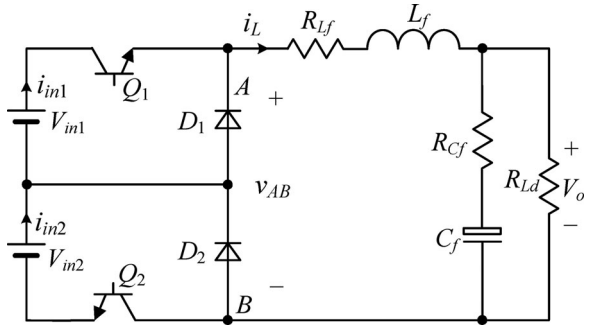

Fig. 1. Double-input buck converter (DIBC).

$$I_{\rm in1} = D_{y1}I_L \tag{2}$$

$$I_{\rm in2} = D_{y2}I_L \tag{3}$$

where D_{y1} and D_{y2} are duty cycles of Q_1 and Q_2 at steady state, respectively, $I_{\rm in1}$ and $I_{\rm in2}$ are the average values of the input currents of the two sources, respectively, and I_L is the average value of the inductor current.

Because there are two duty cycles, besides the output voltage, another variable could be regulated. This provides the possibility of achieving power management. The power management of the DIBC includes the output voltage regulation and the input power distribution over the two input sources. For example, in a hybrid PV–fuel cell system, the solar energy is a renewable energy that serves as the main power source, while fuel cell is the backup power source. The objective of the power management is that the demanded power of the load should be provided by PV arrays as much as possible and the rest are provided by fuel cell.

In this paper, the PV arrays are defined as input source 1, which is the main power source, and the backup power source, such as fuel cell or commercial grid is defined as input source 2. Suppose that the demanded load power is P_o and the available power of input source 1 is $P_{1\max}$, two operating modes of DIBC are defined as follows.

Operating mode I: When $P_{1\max} < P_o$, the two input sources power the load simultaneously. This implies that input source 1 operates under MPPT control to provide maximum power $P_{1\max}$, while input source 2 regulates the output voltage and thus provide the rest of the demanded load power.

Operating mode II: When $P_{1\max} > P_o$, the load power is provided by input source 1, and input source 2 is shut down. This implies that input source 1 regulates the output voltage, so the input power of the source 1 is determined by the demanded power of the load instead of the MPPT controller.

III. OCC for a DIBC

According to the power management and the operating modes defined previously, the implementation of the OCC for DIBC is given as follows.

A. OCC in Operating Mode I

In operating mode I, two duty cycles of the DIBC are used to regulate the input current of source 1 $i_{\rm in1}$ and the output voltage

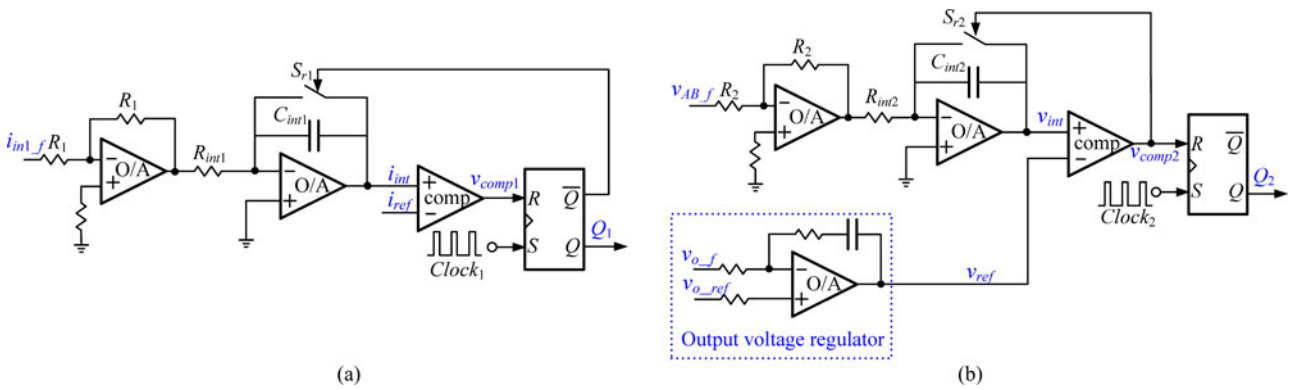

Fig. 2. Control circuit of OCC controllers in operating mode I. (a) OCC controller of $i_{\mathrm{in}1}$. (b) OCC controller of v_{AB}.

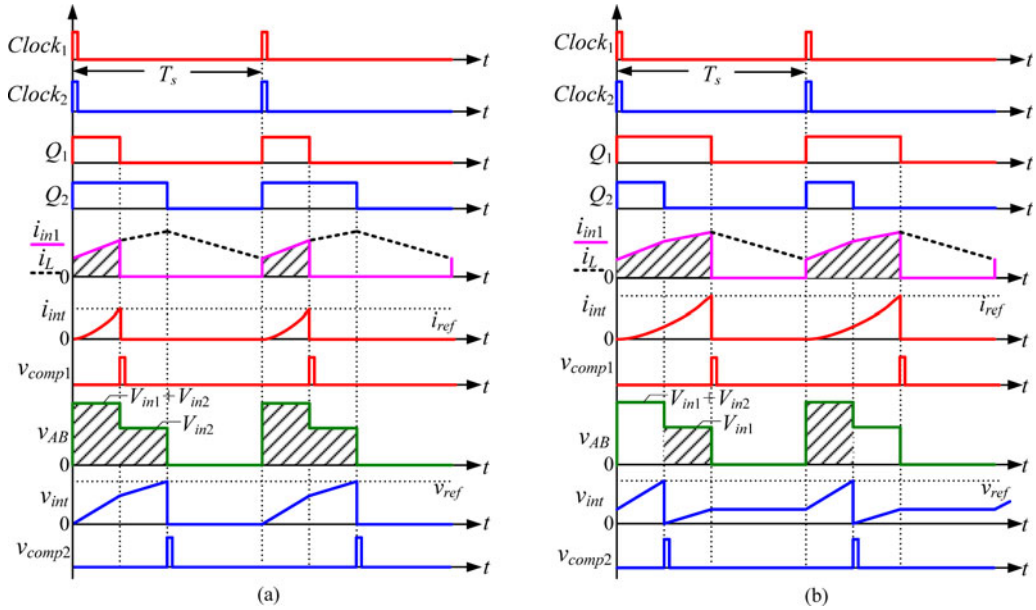

Fig. 3. Key waveforms of OCC controllers in operating mode I. (a) $d_{y1} < d_{y2}$. (b) $d_{y1} > d_{y2}$.

v_o. According to (2), $i_{\mathrm{in}1}$ can only be controlled by d_{y1}. So, d_{y2} is assigned to regulate the output voltage. The control circuits of the OCC controllers are shown in Fig. 2, and the key waveforms are shown in Fig. 3.

1) OCC Controller of $i_{\mathrm{in}1}$: As shown in Fig. 2(a), the OCC controller of $i_{\mathrm{in}1}$ consists of an integrator, an inverter, a comparator, a RS flip-flop, and a reset switch, where $i_{\mathrm{in}1\_f}$ is the sensed input current of the source 1 and the senor gain is k_{if}. A constant frequency clock turns ON Q_1 at the beginning of each switching cycle and activates the integrator simultaneously. Thus, $i_{\mathrm{in}1}$ is integrated, i.e.,

$$i_{\mathrm{int}}(t) = \frac{1}{R_{\mathrm{int}1}C_{\mathrm{int}1}}\int_t k_{if} i_L(t)\,dt. \tag{4}$$

The integral value i_{int} grows from zero, and when it reaches the control reference i_{ref}, the comparator changes its state and resets the RS flip-flop, and turns Q_1 OFF. S_{r1} is turned ON at the same time, and the integrator is reset to zero. S_{r1} is kept ON until the next clock comes. The average value of $i_{\mathrm{in}1}$ in one switching cycle is

$$\langle i_{\mathrm{in}1}\rangle_{T_s} = \frac{1}{T_s}\int_0^{d_{y1}T_s} i_L(t)\,dt = k_i i_{\mathrm{ref}} \tag{5}$$

where $k_i = R_{\mathrm{int}1}C_{\mathrm{int}1}/(k_{if}T_s)$, and T_s is the switching period.

Equation (5) indicates that the average value of $i_{\mathrm{in}1}$ exactly follows its control reference in a switching cycle. This means that OCC not only rejects perturbations from its own input source, but also totally rejects all the perturbations of the other input source, load current, and duty cycle d_{y2}. Moreover, no current regulator is required.

It is noted that the input current reference i_{ref} is obtained from the MPPT controller. However, it is out of the scope of this paper, and is not discussed here.

2) OCC Controller of v_{AB}: As seen in Fig. 1, the average value of the voltage across points *A* and *B* v_{AB} is equal to the output voltage if the voltage drop of the filter inductor is neglected, so v_{AB} is chosen as the controlled variable to regulate the output voltage indirectly. As v_{AB} is determined both by d_{y1} and d_{y2}, if v_{AB} is only integrated when the switch Q_2 is

conducting, the integral value does not represent the average value of v_{AB}. For the integrality of integration of v_{AB}, it is necessary to activate the integration immediately after the integrator being reset at the turn-OFF of Q_2. The circuit of OCC controller of v_{AB} is shown in Fig. 2(b), where v_{AB_f} is the sensed signal of v_{AB}, and the sensor gain is k_{vf}. Unlike the OCC controller of $i_{\text{in}1}$, the reset signal of the integrator is the output of the comparator, which is a narrow pulse signal.

The constant frequency clock turns ON Q_2 at the beginning of each switching cycle. The integrator for v_{AB} is activated at the turn OFF instant of Q_2 in the last switching cycle. Thus, v_{AB} is integrated, i.e.,

$$v_{\text{int}}(t) = \frac{1}{R_{\text{int}2}C_{\text{int}2}} \int_t k_{vf} v_{AB}(t)\, dt. \tag{6}$$

When the integral value v_{int} reaches the control reference v_{ref}, the comparator changes its state and turns Q_2 OFF, and the integrator is reset to zero at the same time. Because the reset signal is a pulse with very short width, the reset time is very short, and the integration is activated immediately after the resetting. Thus, we have

$$\langle v_{AB} \rangle_{T_s} = \frac{1}{T_s} \int_{d_{y2}T_s}^{(1+d_{y2})T_s} v_{AB}(t)\, dt = k_v v_{\text{ref}} \tag{7}$$

where $k_v = R_{\text{int}2}C_{\text{int}2}/(k_{vf}T_s)$.

Equation (7) indicates that the average value of v_{AB} exactly follows its control reference in a switching cycle. Specifically, not only does it rejects perturbations from its own input sources, but also totally rejects all the perturbations of the other input source, load current, and the duty cycle of d_{y1}.

The output voltage v_o is not the actual average value of v_{AB} due to the voltage drop across the filter inductor, so a voltage regulator is necessary to guarantee well-regulated output voltage. The voltage reference of this regulator is v_{o_ref} and its output v_{ref} serves as the reference for the OCC controller of v_{AB}.

B. OCC in Operating Mode II

In operating mode II, the output power is only provided by input source 1, and input source 2 is shut down. In other words, Q_2 is turned OFF, d_{y2} is equal to zero, and the OCC controller of v_{AB} takes over the control of the switch Q_1 instead of the OCC controller of $i_{\text{in}1}$ in operating mode I. The circuit of the OCC controller in operating mode II and the key waveforms are shown in Fig. 4, which is similar to the OCC controller of v_{AB} in operating mode I, and the only difference is that the output of the controller is used to control d_{y1}.

C. Mode Transitions

As can be seen in Figs. 3 and 4, the two switches are controlled by different OCC controllers in different operating modes, so the mode transition circuit is required. The simplest method is to add a multiplexer, as shown in Fig. 5. When the enable signal of the multiplexer EN is low, $Ao = AX$, $Bo = BX$, so the switch Q_1 is controlled by the OCC controller of $i_{\text{in}1}$ and the switch Q_2 is controlled by the OCC controller of v_{AB}. When the enable signal EN goes high, $Ao = AY$, $Bo = BY$; at this time, the switch

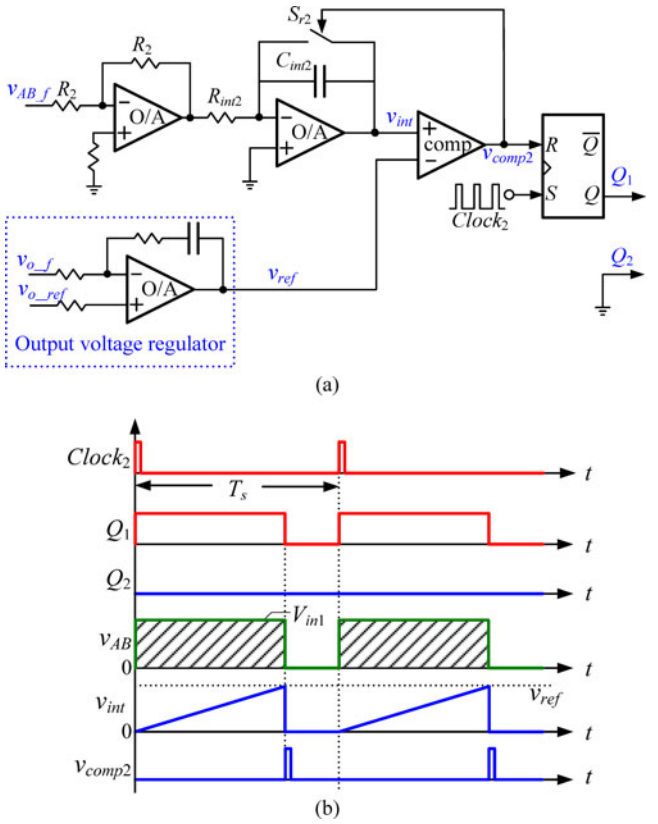

Fig. 4. Control circuit and key waveforms of OCC controller in operating mode II. (a) Control circuit. (b) Key waveforms.

Q_1 is controlled by the OCC controller of v_{AB} and the switch Q_2 is shut down completely.

The key issue is how to select the appropriate control signal to change the state of EN to realize seamless mode transition, according to the available renewable energy and the output power. Because the output voltage of the DIBC is kept constant, v_{ref}, the output of the voltage regulator at the steady state is the same in different operating modes. When $P_{1\max} < P_o$, the DIBC is operated in operating mode I. If the available power of the input source 1 increases or the load current reduces suddenly, which leads to $P_{1\max} > P_o$, the output voltage will increase, and thus, the output of the voltage regulator v_{ref} will keep on reducing until the DIBC is switched to operating mode II. Then the output voltage is regulated to reduce to the reference, and v_{ref} also restores to its steady-state value V_{ref}, which is proportional to the output voltage. Similarly, when $P_{1\max} > P_o$, the DIBC is operated in operating mode II, if the available power of the input source 1 falls or the load current increases, which makes $P_{1\max} < P_o$, the output voltage will keep on reducing, and thus, the output of the voltage regulator v_{ref} will keep on increasing, until the DIBC is switched to operating mode I. Then the output voltage is regulated to increase to the reference, and v_{ref} also restores to its steady-state value V_{ref}.

From the aforementioned analysis, it is known that the output of the voltage regulator v_{ref} will experience a very short downward pulse when the DIBC changes from operating mode I to operating mode II. On the contrary, v_{ref} will experience a

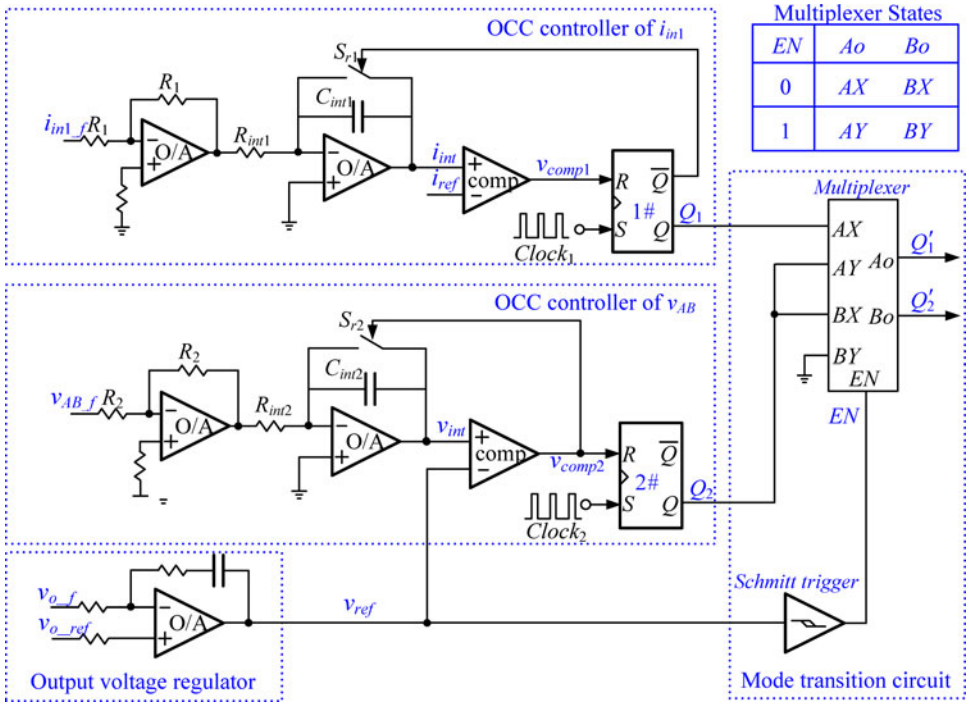

Fig. 5. OCC circuit with multiple operating modes.

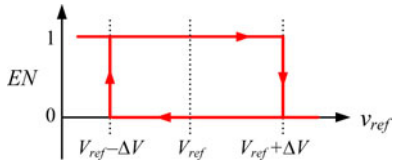

Fig. 6. Characteristic of the Schmitt trigger.

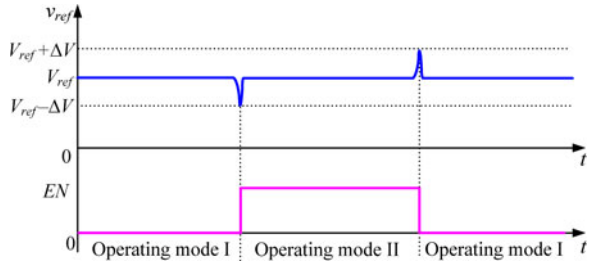

Fig. 7. Transient of $v_{\rm ref}$ during the mode transition.

very short upward pulse when the DIBC changes from operating mode II to operating mode I. According to this, the enable signal EN can be obtained by sending $v_{\rm ref}$ to a Schmitt trigger, as shown in Fig. 5. The center and width of the hysteresis are set at $V_{\rm ref}$ and ΔV, respectively, as shown in Fig. 6. After adopting the Schmitt trigger, EN remains low in operating mode I and high in operating mode II at steady state due to setting of the hysteresis width ΔV. During the mode transition, $v_{\rm ref}$ will keep on changing until it reaches the threshold that is determined by ΔV, and this transient behavior helps to change the state of EN, as shown in Fig. 7. It can be seen that this transient behavior is not sensitive to the value of ΔV. In other words, $v_{\rm ref}$ can always touch the threshold no matter how much the value of ΔV is. As for the case in this paper, ΔV is set at 2 V.

IV. Modeling of a DIBC and Closed-Loop Design

As illustrated in Section III, the DIBC has two operating modes, and the corresponding control loops are different. This section derives the small signal models of the DIBC in the two operating modes.

In operating mode I, the two input sources deliver the power to the load simultaneously. Suppose every variable operates around the steady-state point with a small signal perturbation, i.e., $\langle i_{\rm in1}\rangle_{T_s} = I_{\rm in1} + \hat{i}_{\rm in1}$, $\langle i_{\rm ref}\rangle_{T_s} = I_{\rm ref} + \hat{i}_{\rm ref}$, $\langle v_{AB}\rangle_{T_s} = V_{AB} + \hat{v}_{AB}$, $\langle v_{\rm ref}\rangle_{T_s} = V_{\rm ref} + \hat{v}_{\rm ref}$, and substituting them into (5) and (7) gives

$$\hat{i}_{\rm in1}(s) = k_i \hat{i}_{\rm ref}(s) \tag{8}$$

$$\hat{v}_{AB}(s) = k_v \hat{v}_{\rm ref}(s). \tag{9}$$

From Fig. 1, the relationship between $\hat{v}_{AB}(s)$ and $\hat{v}_o(s)$ can be derived as

$$\hat{v}_o(s) = \hat{v}_{AB}(s)\frac{Z_{Ld}(s)}{sL_f + R_{Lf} + Z_{Ld}(s)} \tag{10}$$

where $Z_{Ld}(s) = ((R_{Ld}[R_{Cf} + 1/(sC_f)])/(R_{Ld} + R_{Cf} + 1/(sC_f)))$.

From (8) to (10), the small signal model of DIBC in operating mode I can be derived, as shown in Fig. 8(a), where $G_{vr}(s)$ is the transfer function of the output voltage regulator and k_f is the output voltage sensor gain. This indicates clearly that $i_{\rm in1}$ is

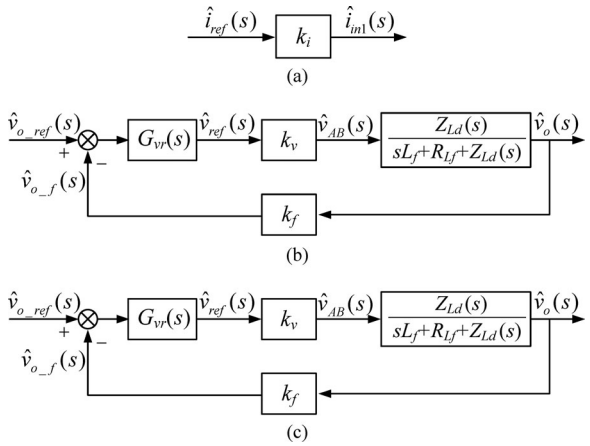

Fig. 8. Small signal models. (a) Operating mode I. (b) Operating mode II.

independent of $v_{\rm ref}$, and the output voltage v_o is independent of $i_{\rm ref}$.

In operating mode II, the input source 1 powers the load independently and $d_{y2} = 0$. The DIBC is equivalent to a single-input buck converter, and the output of the voltage regulator serves as the reference for the OCC controller of v_{AB} to stabilize the output voltage. The small signal model of DIBC in operating mode II can be derived, as shown in Fig. 8(b).

As can be seen in Fig. 5, no current regulator is required for controlling the input current of the input source 1 when OCC is adopted, and only the output voltage regulator is required to design. It can be seen from Fig. 8 that the output voltage loops of operating modes I and II are the same, and the loop gain is expressed as

$$T(s) = k_v k_f G_{vr}(s) \frac{Z_{Ld}(s)}{sL_f + R_{Lf} + Z_{Ld}(s)}. \quad (11)$$

Because the DIBC needs to provide the rating power to the load both in the two operating modes, the design conditions of the output voltage regulator in different operating modes are the same. The design specifications of the DIBC and the parameters of OCC controllers are listed in Section VI.

As shown in Fig. 9, the uncompensated $T(s)$ has a resonant peak, which is determined by the resonant frequency of L_f and C_f. This resonance causes a sharp phase drop. So the design objective is to boost the low-frequency loop gain to minimize the steady-state error while maintaining a sufficient phase margin. A traditional proportional integral (PI) compensator will be able to handle this. The transfer function of the PI compensator is

$$G_{vr}(s) = k_p + \frac{k_i}{s}. \quad (12)$$

In order to increase the dynamic response, the preferred crossover frequency of the output voltage loop is chosen at 1/10 of the switching frequency, i.e., 10 kHz. Meanwhile, the zero of the PI compensator is set at 1/10 of the resonant frequency to avoid more phase drop at this frequency. The corresponding parameters of the PI compensator are $k_p = 135$ and $k_i = 2.5 \times 10^4$. The compensated loop gain of the output voltage loop is also shown in Fig. 9 with the solid lines. It can be seen that the compensated loop gain has a crossover frequency of 10 kHz with a phase margin of 76°.

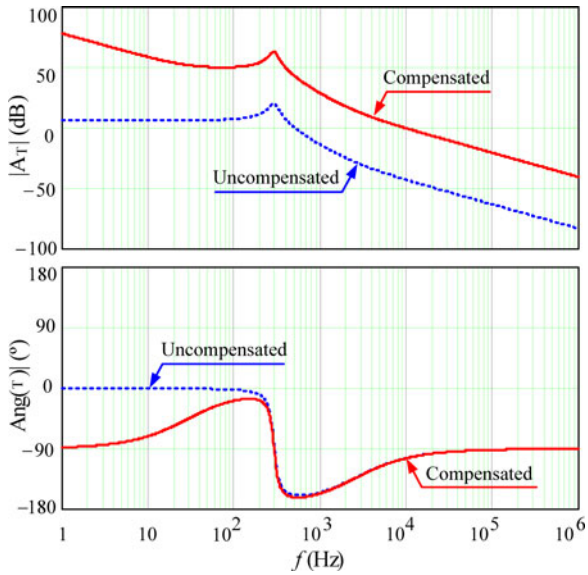

Fig. 9. Output voltage loop gain in operating modes I and II.

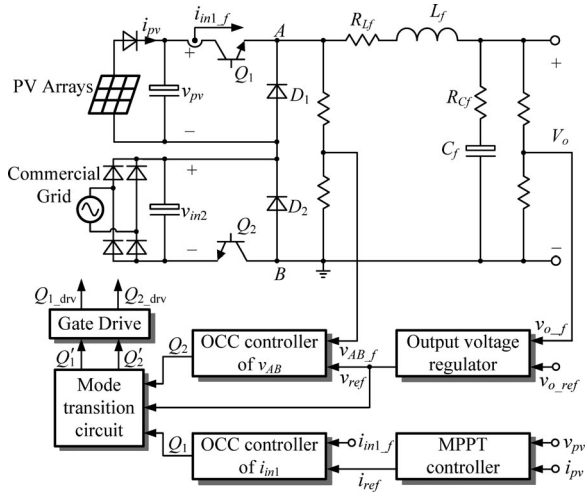

Fig. 10. Block diagram of the whole experimental system.

V. Experimental Results

An 800-W prototype of the DIBC has been built to verify the effectiveness of the proposed OCC method and the design of the output voltage regulator. PV arrays and the rectified commercial grid serve as the main power source and the backup power source, respectively. The block diagram of the whole experimental system is shown in Fig. 10.

The specifications of the prototype are listed as follows.

1) Input source 1: PV arrays formed by eight series-connected SUNTECH solar panels with rated short-circuit current 5 A, open-circuit voltage 350 V, and maximum output power 950 W. The input voltage $V_{\rm in1} = 200$–$350\ V_{\rm DC}$.

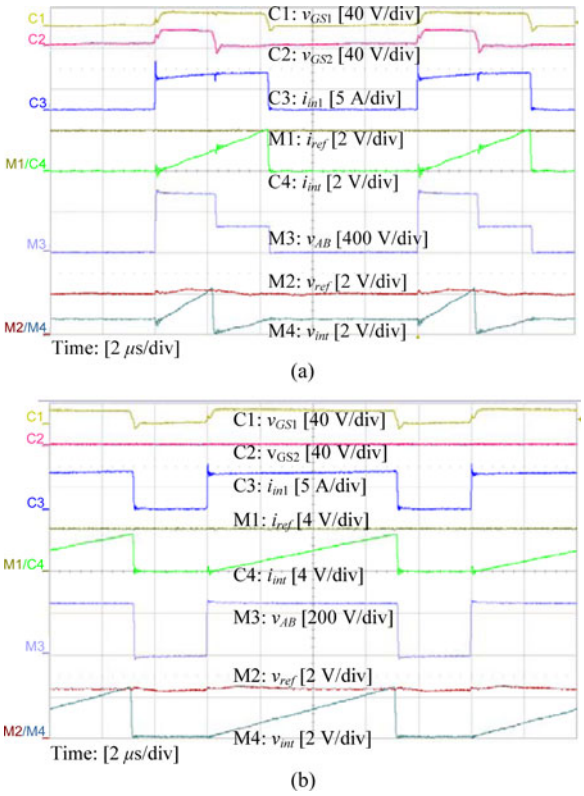

Fig. 11. Experimental waveforms under (a) operating mode I and (b) operating mode II.

2) Input source 2: Rectified 220 V_{AC}/50 Hz commercial grid with $\pm 10\%$ voltage variations. The input voltage $V_{in2} = 311\ V_{DC} \pm 10\%$.
3) Output voltage: $V_o = 180\ V_{DC}$.
4) Output power: $P_o = 800$ W.
5) Switching frequency: $f_s = 100$ kHz.

The key power components and the parameters of OCC controllers are listed as follows.

1) Output filter inductor: $L_f = 1.38$ mH with $R_{Lf} = 0.2\ \Omega$.
2) Output filter capacitor: $C_f = 220\ \mu$F with $R_{Cf} = 0.29\ \Omega$.
3) Integration factor of OCC controller of v_{AB}: $k_v = 70$.
4) Integration factor of OCC controller of i_{in1}: $k_i = 1$.
5) Sensor gain of output voltage: $k_f = 0.03$.

A. Verification of the Steady State of OCC

Fig. 11 shows the experimental waveforms of the gate driving signals, input current of input source 1, the current reference i_{ref}, the integration signal i_{int}, voltage across points A and B v_{AB}, the voltage reference v_{ref}, and its integration signal v_{int}.

Fig. 11(a) shows the experimental waveforms of operating mode I when $P_o < P_{1max}$ and the two input sources deliver the power to the load simultaneously. It can be seen that i_{in1} is integrated when the switch Q_1 is conducting and the integration signal i_{int} is reset immediately when it reaches the current reference i_{ref}. So, the average value of the input current of input source 1 is exactly equal to i_{ref}. Similarly, v_{AB} is integrated during the turn-OFF of Q_2 and the integral value v_{int} is reset when it reaches the voltage reference v_{ref}, and meanwhile, the integration is activated again immediately. So the average value of v_{AB} is exactly equal to v_{ref}. Because v_{ref} is provided by the output voltage regulator, it contains some variations to regulate the output voltage. Fig. 11(b) shows the experimental waveforms of operating mode I when $P_o > P_{1max}$ and the load power is provided by input source 1, while input source 2 is shut down. It can be seen that Q_2 is shut down completely and the OCC controller of v_{AB} takes over the control of the switch Q_1 instead of the OCC controller of i_{in1}. Likewise, v_{AB} is integrated during the turn-OFF of Q_1 and the integral value v_{int} is reset when it reaches the voltage reference v_{ref}, and meanwhile, the integration is activated again immediately. However, the OCC controller of i_{in1} does not control any subject at this time. This verifies that the operating principles of the OCC controllers are correct.

B. Verification of the Dynamic Response of OCC

In order to verify that the interaction of control loops can be eliminated by applying the proposed OCC, the experimental waveforms of load step and P_{1max} step are given, respectively. For a comparison, the dynamic responses of the DIBC with the traditional linear feedback control method used in [13] are also measured under the same conditions.

Fig. 12 shows that the output power steps between 700 and 800 W when P_{1max} keeps constant at 500 W. It can be seen that the average value of input current of input source 1 is interfered by regulation of the output voltage loop under the traditional linear feedback control when the load current steps, as shown in Fig. 12(a), while it keeps constant under the proposed OCC control, as shown in Fig. 12(b). Fig. 13 shows that the P_{1max} steps between 400 and 500 W at the full load 800 W, when the MPPT controller regulates i_{ref} to trace the maximum power. In order to observe the dynamic response more clearly, the output voltage is shown in an ac coupled manner. The output voltage is interfered by the regulation of the input current loop under the traditional control due to the effect of the cross-coupling transfer functions, as shown in Fig. 13(a). And because the average value of v_{AB} can be regulated in one switch cycle under OCC control, the output voltage is not influenced by the change of input current of input source 1, as shown in Fig. 13(b). From Figs. 12 and 13, it can be seen clearly that the interaction of the current and voltage loops is diminished by the OCC control.

C. Verification of Seamless Mode Transition

In order to verify that the DIBC can transit between the two operating modes automatically according to the available renewable energy and the output power, the experimental results are shown in Fig. 14(a) and (b) when the load step and P_{1max} step, respectively, are intentionally imposed.

Fig. 14(a) shows the dynamic response of the DIBC when the load current steps down and up between full load (4.44 A) and half load (2.22 A), and P_{1max} keeps constant at 500 W. When the DIBC operates at full power, i.e., $P_{1max} < P_o$, the PV arrays output the maximum power and the corresponding output current i_{in1} is 2 A, meanwhile the commercial grid provides the rest power. When the load current steps down to the half load of 2.22 A suddenly, which makes $P_{1max} > P_o$, the output voltage

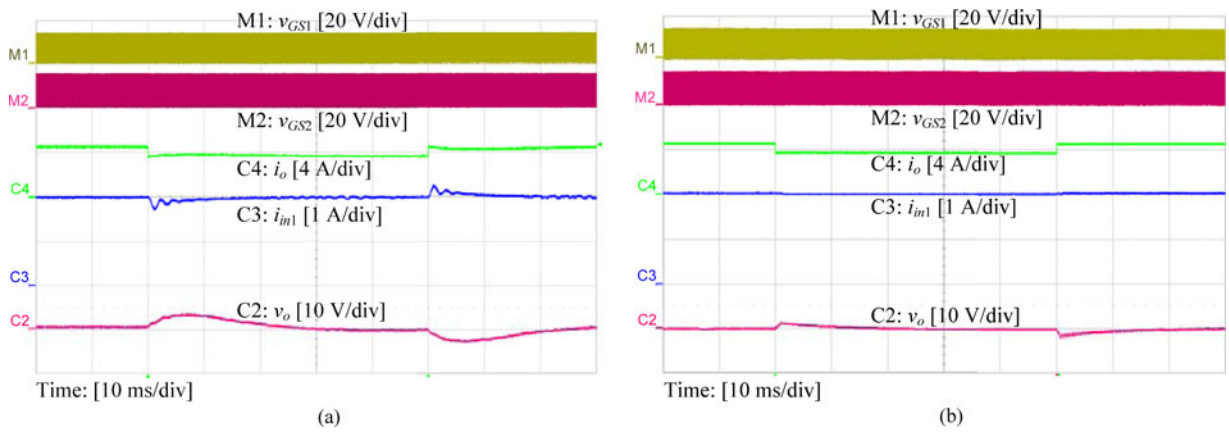

Fig. 12. Experimental waveforms corresponding to a step change in load current when $P_{1\max} = 500\,\text{W}$ (a) with linear feedback control and (b) with OCC control.

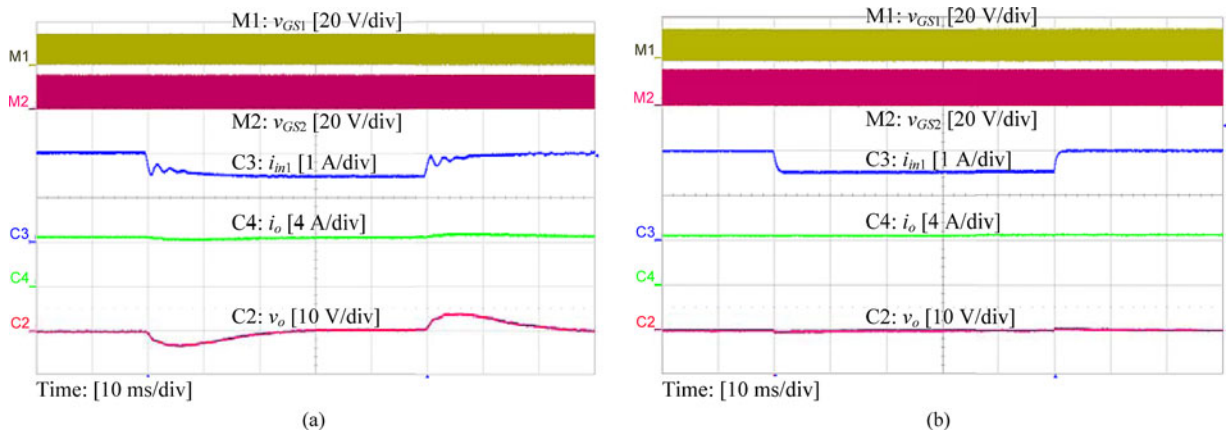

Fig. 13. Experimental waveforms corresponding to a step change of $P_{1\max}$ at full load (a) with linear feedback control and (b) with OCC control.

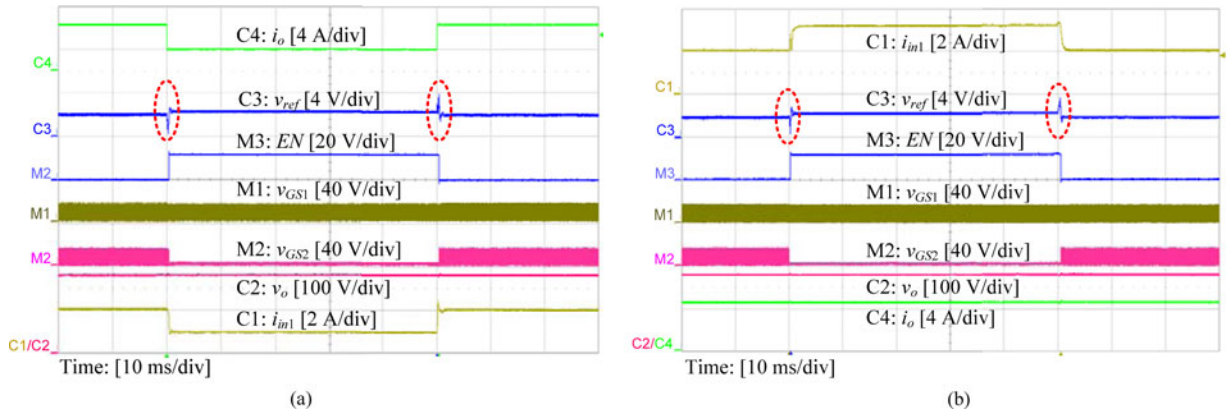

Fig. 14. Experimental waveforms of mode transition corresponding to (a) a step change of load current and (b) a step change of $P_{1\max}$.

increases due to the excess input power. So, the output of the voltage regulator v_{ref} keeps on decreasing until it reaches the under threshold voltage of the Schmitt trigger. As a result, EN changes from low to high and switches the DIBC from operating mode I to II, and after a very short time, v_{ref} restores to its steady-state V_{ref} which is proportional to the output voltage, as marked by dashed cycle. At this time Q_2 is shut down, and the PV arrays are controlled to regulate the output voltage and power the load individually. The corresponding average value of the input current i_{in1} is 1 A. When the load steps back to the full load, which makes $P_{1\max} < P_o$, the output voltage decreases due to insufficient input power. So, the output of the voltage regulator v_{ref} keeps on increasing until it reaches the upper threshold voltage of the Schmitt trigger. As a result, EN changes from high to low and switches the DIBC from operating mode II to operating mode I, after a very short time, v_{ref} restores

to its steady-state $V_{\rm ref}$. At this time, the PV arrays provide the maximum power again and the commercial grid provides the rest of the demanded load power. During the load steps, the output voltage is kept at the 180 V constantly.

Fig. 14(b) shows the dynamic response of the DIBC when $P_{1\max}$ steps between 500 and 900 W at the full load. When the DIBC operates at the rating power, $P_{1\max} < P_o$, so the PV arrays output at the maximum power and the corresponding output current $i_{\rm in1}$ is 2 A, meanwhile the commercial grid provides the rest power. When $P_{1\max}$ steps up to 900 W, which makes $P_{1\max} > P_o$, the output voltage increases due to the excess input power. So, the output of the voltage regulator $v_{\rm ref}$ keeps on falling until it reaches the under threshold voltage of the Schmitt trigger. As a result, EN changes from low to high and switches the DIBC from operating mode I to II, and after a very short time, $v_{\rm ref}$ restores to its steady-state $V_{\rm ref}$ which is proportional to the output voltage, as marked by the dashed cycle. At this time Q_2 is shut down, and the PV arrays are controlled to regulate the output voltage and power the load individually. The corresponding average value of the input current $i_{\rm in1}$ is 3.6 A. When $P_{1\max}$ steps back to 500 W, and makes $P_{1\max} < P_o$, the output voltage decreases due to insufficient input power. So, the output of the voltage regulator $v_{\rm ref}$ keeps on increasing until it reaches the upper threshold voltage of the Schmitt trigger. As a result, EN changes from high to low and switches the DIBC from operating mode II to I, after a very short time, $v_{\rm ref}$ restores to its steady-state $V_{\rm ref}$, as marked by dashed cycle. At this time, the PV arrays provide the maximum power again and the commercial grid provides the rest of the demanded load power. During $P_{1\max}$ steps, the output voltage is kept at the 180 V constantly.

It should be noted that reset delay of the integrator is inevitable in OCC controllers. So in operating mode I, there is an integration loss when v_{AB} is not zero during the reset period, as shown in Fig. 11(a). This error is corrected by the output voltage regulator, and thus, a minor adjustment of steady-state value of $v_{\rm ref}$ can be observed between the two operating modes.

This reveals that the mode transition circuit can realize seamless mode transition according to the available renewable energy and the output power.

VI. Conclusion

In hybrid power systems, the use of an MIC instead of several single-input converters has the advantages of simpler circuit and lower cost. However, the MIC is a typical multiple-input multiple-output coupling system and has many operating modes under the power management strategy, so the closed-loop design is very complicated.

Taking the DIBC as an example, this paper proposes an OCC method for MIC to eliminate the interactions of the coupling loops and, thus, to simplify the control design. The OCC control circuits in different operating modes are implemented, and the mode transition is discussed in detail. The small signal models of the DIBC for different operating modes are derived separately. It can be seen that with OCC, no current regulator is required, and the design conditions of the output voltage regulator in different operating modes are the same. As a result, the control design is greatly simplified. An 800-W prototype has been built and tested in the lab, and the experimental results validate the steady state and dynamic performances of the proposed OCC.

References

[1] S. K. Kim, J. H. Jeon, C. H. Cho, J. B. Ahn, and S. H. Kwon, "Dynamic modeling and control of a grid-connected hybrid generation system with versatile power transfer," *IEEE Trans. Ind. Electron.*, vol. 55, no. 4, pp. 1677–1688, Apr. 2008.

[2] C. S. Wang and M. H. Nehrir, "Power management of a stand-alone wind/photovoltaic/fuel cell energy system," *IEEE Trans. Energy Convers.*, vol. 23, no. 3, pp. 957–967, Sep. 2008.

[3] F. Valenciaga and P. F. Puleston, "Supervisor control for a stand alone hybrid generation system using wind and photovoltaic energy," *IEEE Trans. Energy Convers.*, vol. 20, no. 2, pp. 398–405, Jun. 2005.

[4] Y. M. Chen, Y. C. Liu, and S. H. Lin, "Double-input PWM dc–dc converter for high/low voltage sources," *Ind. Electron.*, vol. 53, no. 5, pp. 1538–1544, Oct. 2006.

[5] Z. J. Qian, O. Abdel-Rahman, and I. Batarseh, "An integrated four-port dc–dc converter for renewable energy applications," *IEEE Trans. Power Electron.*, vol. 25, no. 7, pp. 1877–1887, Jul. 2010.

[6] Y. C. Liu and Y. M. Chen, "A systematic approach to synthesizing multiple-input dc–dc converters," *IEEE Trans. Power Electron.*, vol. 24, no. 1, pp. 116–127, Jan. 2009.

[7] Y. Li, X. B. Ruan, D. S. Yang, F. X. Liu, and C. K. Tse, "Synthesis of multiple-input dc/dc converters," *IEEE Trans. Power Electron.*, vol. 25, no. 9, pp. 2372–2385, Sep. 2010.

[8] Y. M. Chen, Y. C. Liu, F. Y. Wu, and Y E. Wu, "Multi-input converter with power factor correction and maximum power point tracking features," in *Proc. 17th Annu. IEEE Appl. Power Electron. Conf. Expo.*, 2002, pp. 490–496.

[9] L. Solero, A. Lidozzi, and J. A. Pomilio, "Design of multiple-input power converter for hybrid vehicles," *IEEE Trans. Power Electron.*, vol. 20, no. 5, pp. 1007–1016, Sep. 2005.

[10] N. D. Benavides and P. L. Chapman, "Power budgeting of a multiple-input buck-boost converter," *IEEE Trans. Power Electron.*, vol. 20, no. 6, pp. 1303–1309, Nov. 2005.

[11] Y. M. Chen, Y. C. Liu, S. C. Hung, and C. S. Cheng, "Multi-input inverter for grid-connected hybrid PV/wind power system," *IEEE Trans. Power Electron.*, vol. 22, no. 3, pp. 1070–1077, May 2007.

[12] D. Somayajula and M. Ferdowsi, "Small-signal modeling and analysis of the double-input buck-boost converter," in *Proc. 25th Annu. IEEE Appl. Power Electron. Conf. Expo.*, 2010, pp. 2111–2115.

[13] V. Mummadi and K. K. Sawant, "Control of multi-input integrated buck-boost converter," in *Proc. 3rd Int. Conf. Ind. Inf. Syst.*, Dec. 2008, pp. 1–6.

[14] Y. Li, X. Ruan, D. Yang, and F. Liu, "Modeling, analysis and design for hybrid power systems with dual-input dc–dc converter," in *Proc. IEEE Energy Convers. Congr. Expo.*, 2009, pp. 3203–3210.

[15] Z. J. Qian, O. Abdel-Rahman, H. Al-Atrash, and I. Batarseh, "Modeling and control of three-port dc–dc converter interface for satellite applications," *IEEE Trans. Power Electron.*, vol. 25, no. 3, pp. 637–649, Mar. 2010.

[16] D. W. Liu, H. Li, and L. D. Marlino, "Design of a 6 kW multiple-input bi-directional dc–dc converter with decoupled current sharing control for hybrid energy storage elements," in *Proc. 22nd Annu. IEEE Appl. Power. Electron. Conf.*, 2007, pp. 509–513.

[17] C. H. Zhao, S. D. Round, and J. W. Kolar, "An isolated three-port bidirectional dc–dc converter with decoupled power flow management," *IEEE Trans. Power Electron.*, vol. 23, no. 5, pp. 2443–2453, Sep. 2008.

[18] K. M. Smedley and C. Slobodan, "One-cycle control of switching converters," *IEEE Trans. Power Electron.*, vol. 10, no. 6, pp. 625–633, Nov. 1995.

[19] G. Z. Chen and K. M. Smedley, "A current source with one-cycle control and its application in serial hybrid active power filter," in *Proc. 34th Annu. IEEE Power Electron. Spec. Conf.*, 2003, pp. 797–802.

[20] K. M. Smedley and C. Slobodan, "Dynamics of one-cycle controlled Cuk converters," *IEEE Trans. Power Electron.*, vol. 10, no. 6, pp. 634–639, Nov. 1995.

[21] Z. R. Lai and K. M. Smedley, "A new extension of one-cycle control and its application to switching power amplifiers," *IEEE Trans. Power Electron.*, vol. 11, no. 1, pp. 99–105, Jan. 1996.

[22] Z. R. Lai, K. M. Smedley, and Y. H. Ma, "Time quantity one-cycle control for power-factor correctors," *IEEE Trans. Power Electron.*, vol. 12, no. 2, pp. 369–375, Mar. 1997.

[23] C. M. Qiao, T. T. Jin, and K. M. Smedley, "One-cycle control of three-phase active power filter with vector operation," *IEEE Trans. Power Electron.*, vol. 51, no. 2, pp. 455–463, Apr. 2004.
[24] Y. Chen and K. M. Smedley, "A cost-effective single-stage inverter with maximum power point tracking," *IEEE Trans. Power Electron.*, vol. 19, no. 5, pp. 1289–1294, Sep. 2004.

Dongsheng Yang was born in Jiangsu, China, in 1984. He received the B.S. and M.S. degrees in electrical engineering and automation from the Nanjing University of Aeronautics and Astronautics, Nanjing, China, where he is currently working toward the Ph.D. degree in electrical engineering.

His main research interests include renewable energy systems and grid-connected inverter.

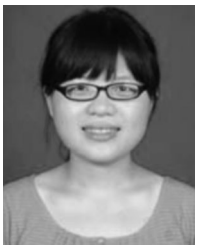

Min Yang was born in Jiangsu, China, in 1987. She received the B.S. degree in electrical engineering and automation from the Nanjing University of Aeronautics and Astronautics, Nanjing, China, in 2010, where she is currently working toward the M.S. degree in electrical engineering.

Her main research interests include one-cycle control, multiple-input converter, and dual active bridge.

Xinbo Ruan (M'97–SM'02) was born in Hubei, China, in 1970. He received the B.S. and Ph.D. degrees in electrical engineering from the Nanjing University of Aeronautics and Astronautics (NUAA), Nanjing, China, in 1991 and 1996, respectively.

In 1996, he joined the Faculty of Electrical Engineering Teaching and Research Division, NUAA, and became a Professor in the College of Automation Engineering, NUAA, in 2002, where he has been involved in teaching and research in the field of power electronics. From August to October 2007, he was a Research Fellow in the Department of Electronics and Information Engineering, Hong Kong Polytechnic University, Hong Kong. Since March 2008, he has been with the College of Electrical and Electronic Engineering, Huazhong University of Science and Technology, Wuhan, China. He has published more than 100 technical papers in journals and conferences and also published three books. His main research interests include soft-switching dc/dc converters, soft-switching inverters, power factor correction converters, modeling the converters, power electronics system integration, and renewable energy generation system.

Dr. Ruan was awarded the Delta Scholar by the Delta Environment and Education Fund in 2003, and was awarded the Special Appointed Professor of the Chang Jiang Scholars Program by the Ministry of Education, China, in 2007. He is a Guest Professor of Beijing Jiaotong University, Beijing, China, and the Hefei University of Technology, Hefei, China. Since 2005, he has served as the Vice President of the China Power Supply Society, and since 2008, he has been a member of the Technical Committee on Renewable Energy Systems within the IEEE Industrial Electronics Society. Since 2011, he has been an Associate Editor for the IEEE TRANSACTIONS ON INDUSTRIAL ELECTRONICS. He is a senior member of the IEEE Power Electronics Society and the IEEE Industrial Electronics Society.